In Situ Synthesis of Ni-BTC Metal−Organic Framework@Graphene Oxide Composites for High-Performance Supercapacitor Electrodes

Tianen Chen, Tao Shen, Yuanhao Wang, Zexu Yu, Wei Zhang, Yi Zhang, Zeen Ouyang, Qingguo Cai, Yaxiong Ji,* and Shifeng Wang*
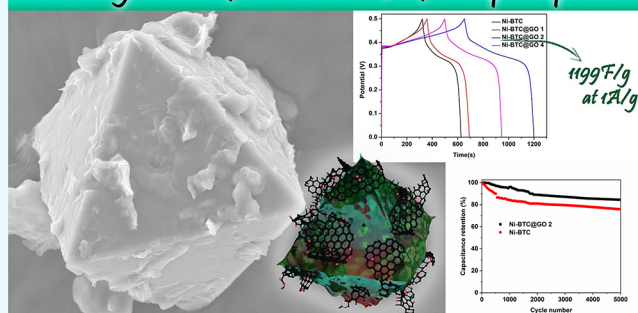
Read Online

ACCESS | Metrics & More | Article Recommendations | Supporting Information

ABSTRACT: In response to serious ecological and environmental problems worldwide, a novel graphene oxide (GO) induction method for the in situ synthesis of GO/metal organic framework (MOF) composites (Ni-BTC@GO) for supercapacitors with excellent performance is presented in this study. For the synthesis of the composites, 1,3,5-benzenetricarboxylic acid (BTC) is used as an organic ligand due to its economic advantages. The optimum amount of GO is determined by a comprehensive analysis of morphological characteristics and electrochemical tests. 3D Ni-BTC@GO composites show a similar spatial structure to that of Ni-BTC, revealing that Ni-BTC could provide an effective framework and avoid GO aggregation. The Ni-BTC@GO composites have a more stable electrolyte−electrode interface and an improved electron transfer route than pristine GO and Ni-BTC. The synergistic effects of GO dispersion and Ni-BTC framework on electrochemical behavior are determined, where Ni-BTC@GO 2 achieves the best performance in energy storage performance. Based on the results, the maximum specific capacitance is 1199 F/g at 1 A/g. Ni-BTC@GO 2 has an excellent cycling stability of 84.47% after 5000 cycles at 10 A/g. Moreover, the assembled asymmetric capacitor exhibits an energy density of 40.89 Wh/kg at 800 W/kg, and it still remains at 24.44 Wh/kg at 7998 W/kg. This material is expected to contribute to the design of excellent GO-based supercapacitor electrodes.

1. INTRODUCTION

Fossil fuels have been the primary source of energy for economic growth since the industrial revolution.[1] On the one hand, utilization of large amounts of fossil fuels, however, has led to serious ecological and environmental issues worldwide, such as air pollution and photochemical smog. On the other hand, as the world's population continues to grow, the demand for energy is increasing, which will inevitably cause an energy crisis.[1,2] Even in the Tibet region of China, which is known as the third pole of the world, the same problem is faced. One thing that should be noticed is that lots of energy resources, including geothermal and solar energy, exist in the plateau areas of China, such as Tibet, Xinjiang, and Inner Mongolia. The conversion of these energy sources into electrical energy and further application in electric vehicles, high-speed rail, and various household electronic devices could be an ideal strategy for pollution control and energy saving.[3−7] Noteworthily, benefiting from rapid charging/discharging speed, high density of power, and long cycle life, supercapacitors are attracting increasing research focus in energy storage systems.[8−13] The preparation of high-performance supercapacitors is highly valued, which is crucial for the development of electrode materials.[14−19]

Compared with traditional carbon materials, recent research studies focus on the investigation of novel two-dimensional materials as an electrode candidate, such as metal oxides, conductive polymers, transition metal carbonitrides, etc.[20−25] Particularly, the application of graphene and its derivatives in supercapacitors has become a hot spot.[26,27] Graphene oxide (GO) has been proved to show excellent electrical conductivity, water permeability, mechanical property, and ultrahigh theoretical specific surface area. In addition, due to the richness of oxygen-containing groups, GO could provide enough active sites for the growth of the material while initiating the Faradaic reaction of supercapacitors.[28,29] Unfortunately, strong directional interactions lead to the accumulation of graphene oxide, limiting active sites and decreasing the specific surface area, thus creating a significant barrier to the application of GO.[30,31]
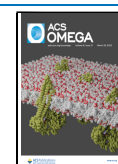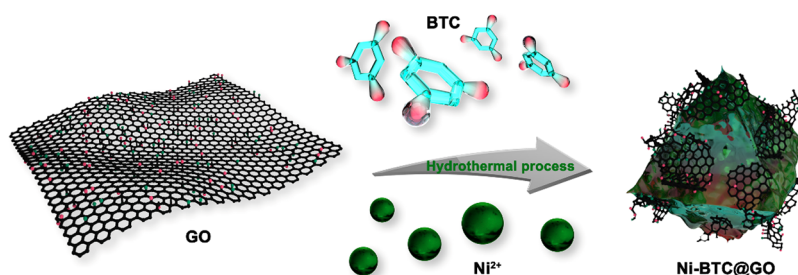
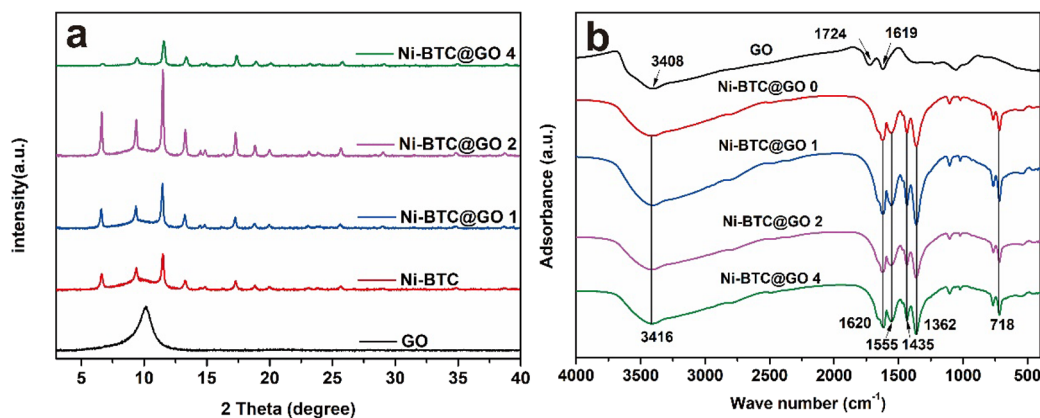**Figure 1.** Preparation process of the Ni-BTC@GO composites.

Figure 2. (a) XRD patterns of GO, Ni-BTC, and Ni-BTC@GO composites; (b) FT-IR spectra of GO, Ni-BTC, and Ni-BTC@GO composites.

Metal−organic frameworks (MOFs) are classified as periodic skeletal materials composed of transition metal ions/clusters and organic moieties. Benefiting from the adjustable pore sizes, diverse structures, and large specific surface area, MOFs are widely used in fields of hydrogen storage, ionic batteries, catalysis, gas adsorption/separation, and supercapacitors.[31−35] Xiao et al. synthesized a nickel-based metal−organic framework $(Ni_2(OH)_2(C_8H_4O_4))$ with a hierarchical microblock structure and used it as the electrode of a supercapacitor, which displayed a specific capacitance of 631 C/g at a current density of 1 A/g.[36] Kale et al. prepared nanoflower-like Ni-MOF and obtained a high specific capacity (C_s) of 467 C/g at 1 A/g.[37] Gao et al. synthesized Ni-MOF and verified a specific capacitance of 804 F/g at 1 A/g.[35] Although a satisfactory specific capacity of Ni-based MOFs is obtained, most of them have poor conductivity, severely limiting actual application as supercapacitors.

To repair the poor electrical conductivity of MOF-based materials, multifunctional MOF heterojunctions are proposed through the synergistic interaction between individual functional units.[38] To prepare high-performance supercapacitor electrodes, Hong et al. synthesized Ni-Co-MOF/GO composites, whose maximum specific capacitance was 447.2 F/g at a current density of 1 A/g.[39] 2D/2D NiCo-MOFs/GO composite nanosheets have a specific capacitance of 413.61 C/g at a current density of 0.5 A/g.[40] Qu et al. synthesized Ni-MOF/Ti_3C_2T_x nanosheets for supercapacitor electrodes, whose specific capacitance is 867.3 F/g at 1 A/g.[41] A synergistic effect between Ni-MOF and GO on electrochemical performance is observed and proposed.[39,42] The presence of GO can solve the issue of poor electrical conductivity of MOFs, while the composites formed by MOFs and GO can reduce or even eliminate the strong directional force between GO and thus prevent the aggregation of GO. The inherent synergistic mechanism and structural optimization of these hybrid materials, however, are still vague so far.[39−41,43]

This paper reports a facile method to prepare Ni-MOF@GO composites to meet the demand for supercapacitors with high performance. 1,3,5-Benzenetricarboxylic acid (H_3BTC) is chosen as the economical organic ligand and nickel nitrate as the metal salt for the in situ synthesis of Ni-BTC@GO composites together with GO. The ultimate goal of this study is to prepare electrode materials with extremely good electron and charge transport characteristics by means of characterizing the morphology of the composites and analyzing their electrochemical properties. Meanwhile, the mechanism by which the composite structured materials increase in conductivity and specific capacitance relative to Ni-BTC itself, as well as the influence of the ratio of Ni-BTC and GO on the specific capacitance of composite structured materials, is also fully investigated.

2. EXPERIMENTAL SECTION

2.1. Synthesis of GO. For preparing GO, the modified Hummer's strategy was used,[44] and the detailed steps are shown in the Supporting Information.

2.2. Synthesis of Ni-BTC. Ni-BTC was prepared in accordance with previously published procedures.[45] $Ni(NO_3)_2\cdot6H_2O$ (912 mg), 1,3,5-trimesic acid (BTC) (435 mg), and 2-methyl-imidazole (117 mg) were sonicated for 30 min in 31.8 mL of DMF. The solution was baked at 170 °C for 48 h in a Teflon-lined autoclave. The crystals were first obtained after being naturally cooled, filtered, washed with DMF and ethanol; after that, drying at 80 °C was processed for 24 h.

2.3. Synthesis of Ni-BTC@GO. Ni-BTC@GO composites are prepared according to Figure 1. GO sheets (0, 10, 20, and 40 mg) in 31.8 mL of DMF were sonicated for 30 min to
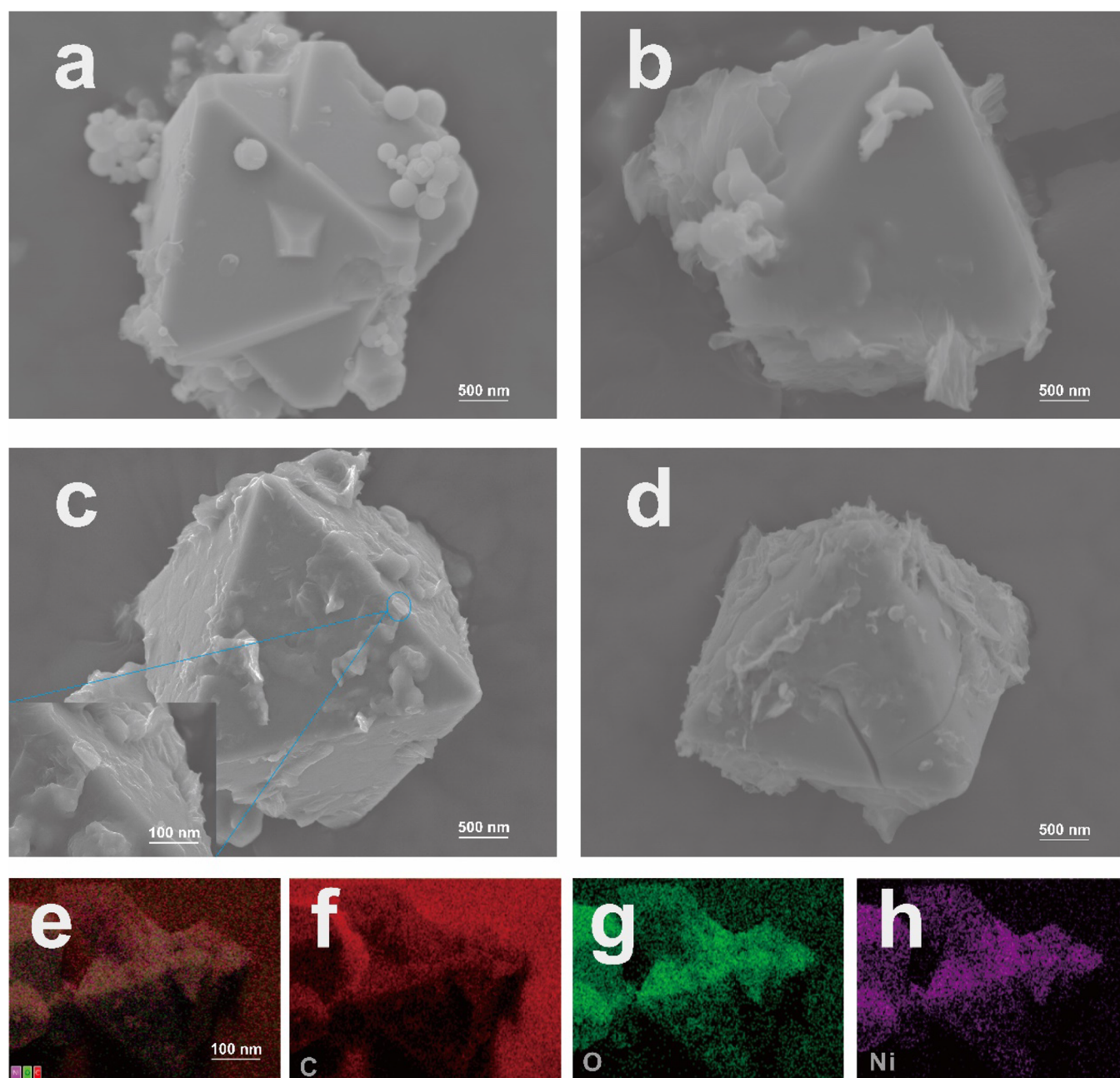
Figure 3. (a−d) SEM images of Ni-BTC@GO 0, 1, 2, and 4; (e−h) EDS mapping of Ni-BTC@GO.

obtain GO that is uniformly distributed, followed by addition of 1,3,5-trimesic acid (BTC) (435 mg), Ni(NO$_3$)$_2$·6H$_2$O (912 mg), and 2-methyl-imidazole (117 mg). The blend was obtained using the same strategy described in Section 2.2. Series hybrid materials were prepared by adjusting the GO dosage (0, 0.01, 0.02, and 0.04 g of GO), which are denoted as Ni-BTC@GO 0, 1, 2, and 4, respectively.

3. RESULTS AND DISCUSSION

3.1. Morphological Characterization. Figure 2a depicts the XRD results of GO, Ni-BTC, Ni-BTC@GO 1, Ni-BTC@GO 2, and Ni-BTC@GO 4. The (001) reflection of GO corresponds to the peak at $2\theta = 10.1°$.[46] Characteristic peaks of Ni-BTC are in complete agreement with the literature.[45] The characteristic peak of GO disappears in the XRD patterns of Ni-BTC@GO composites, which may result from the

following: (i) The greater randomness of GO dispersion on the Ni-BTC surface decreases the aggregation state and orderliness of lamellar GO. (ii) Relatively low GO dosage results in its inconspicuous characteristic peak. To detect the existence of GO in Ni-BTC@GO, the Ni-BTC@GO 2 composites have been ground to completely break the Ni-BTC crystal, and then XRD characterization of the ground composite materials is conducted again; as shown in Figure S1, it can be clearly observed that the characteristic peak of GO appears. This is a strong proof of the existence of GO in Ni-BTC@GO. In the XRD pattern of Ni-BTC@GO 4, the characteristic peak of Ni-BTC becomes less obvious, which is caused by the fact that the excess GO destroys the crystallinity of Ni-BTC.[47] Moreover, the higher peak intensity of Ni-BTC@GO 2 is due to the smaller effect of GO sheets on the crystallinity of Ni-BTC, which could be further observed by SEM and TEM images.
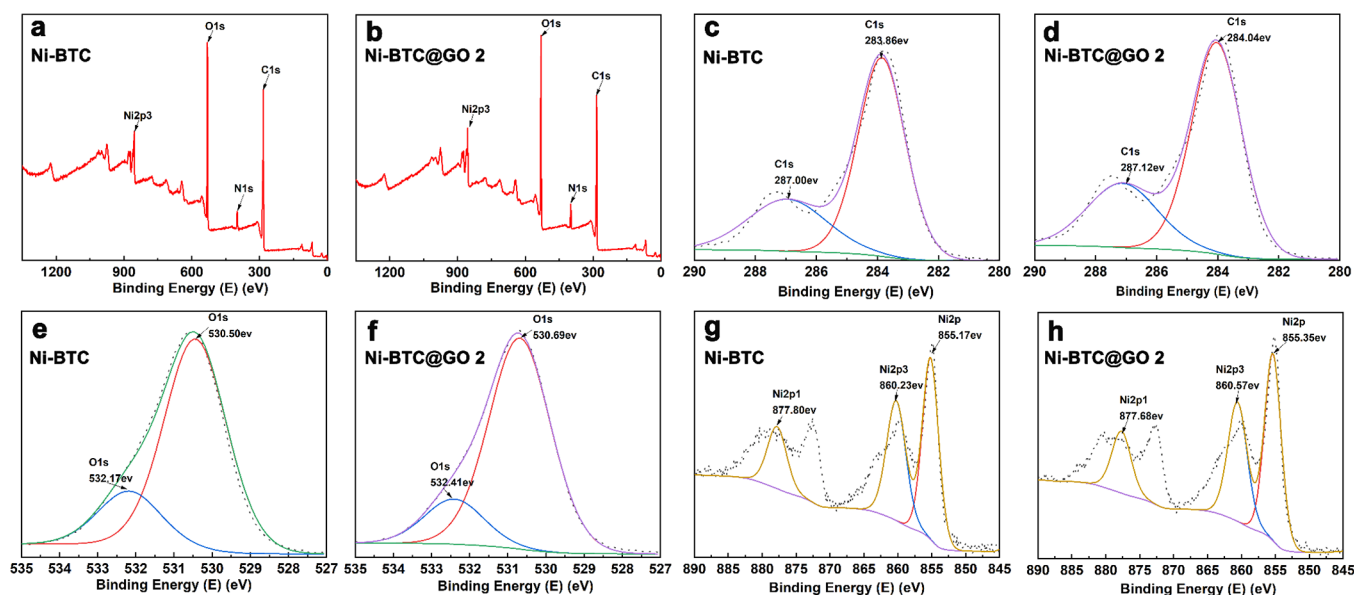
Figure 4. XPS survey spectra of (a) Ni-BTC and (b) Ni-BTC@GO 2 and C1s (c, d), O1s (e, f), and Ni2p (g, h) of Ni-BTC and Ni-BTC@GO 2, respectively.

FT-IR has been used as a powerful tool to characterize the structure of Ni-BTC and Ni-BTC@GO (Figure 2b). The peak at 3408 cm^{-1} is derived from −OH groups.[45] Interactions between GO and Ni-BTC are verified by the slight shift of the C=O stretching mode and ester groups (from 1724 and 1619 cm^{-1} to 1620 and 1555 cm^{-1}).[47] From the spectrum diagram of Ni-BTC@GO composites, C−H stretching and asymmetric bending are observed at 1435 cm^{-1}. Strong absorption bands attributed to the bound C−O group occur at 1435 and 1362 cm^{-1}, indicating that the BTC is coordinated with Ni.[45] An O−H absorption peak at 3416 cm^{-1} reveals that some carboxyl groups are not fully deprotonated, which accounts for some free carboxylates. Finally, the peak at 1637 cm^{-1} confirms the coordination of Ni with −COO− moieties.[39,46]

To further characterize the morphology of the as-prepared composites visually, SEM images are shown in Figure 3. Ni-BTC crystals are uniform octahedral particles with smooth surfaces, the dimensions of which are about 5 μm (Figure 3a).[48] Compared with Ni-BTC, the Ni-BTC@GO materials show similar morphology to Ni-BTC, suggesting the negligible effect of GO on the structure of Ni-BTC. The composites exhibit different phase transitions with significantly rougher surfaces (Figure 3b−d). In addition, the surface of the composites can be clearly observed to be covered with layered materials, and its morphology is consistent with the SEM image of GO (Figure S2). The EDS mapping of Ni-BTC@GO 2 also shows that the C element is uniformly distributed on the surface of the composite (Figure 3f). All these can prove the successful composite of GO and Ni-BTC. At lower GO dosage, it can be clearly seen that GO sheets intermittently disperse on the surface of Ni-BTC, and the sheets could not cover the whole octahedral structure (Figure 3b). A moderate amount of GO can be uniformly dispersed on the surface of Ni-BTC crystals and firmly anchored on it (Figure 3c). Ni-BTC crystals contribute to disorder GO dispersion and effectively solve the problem of GO aggregation (Figure 3b,c). As shown by the EDS mapping of Ni-BTC@GO 2 (Figure 3e−h), the elements C, O, and Ni are uniformly dispersed over the surface of Ni-BTC, demonstrating that GO has been successfully dispersed.

In addition, the existence of Ni demonstrates that GO is partially covered on the particle surface, which can (i) effectively increase the contact area between the electrode and the electrolyte and (ii) shorten the diffusion path of ions and preserve the active site of Ni^{2+} during the electrochemical test. However, high GO dosage in Ni-BTC@GO 4 results in GO aggregation on Ni-BTC, leading to a defective morphology. When compared to Ni-BTC, Ni-BTC@GO 4 has a similar octahedral structure but visible crystal defects. The size of Ni-BTC@GO 4 nanoparticles is similar, but fewer active sites are exposed than Ni-BTC@GO 1 and Ni-BTC@GO 2. GO intervention not only limits the growth of MOF nuclei but also results in GO agglomeration.[47] From the SEM images of Ni-BTC@GO composites, it can be concluded that the GO sheet gradually covers the whole surface of Ni-BTC uniformly with the increase in GO dosage. As flexibility is one of the main characteristics of GO sheets, surplus GO may cause the incorporation between GO sheets and the Ni-BTC surface; as a result, Ni-BTC@GO 4 has a similar crystal structure to Ni-BTC. Results from SEM images are consistent with XRD.

After being decorated with GO sheets, a lower N$_2$ uptake amount is obtained on Ni-BTC@GO 2 than the pristine Ni-BTC (Figure S3), indicating that the coverage of GO would hinder the surface porosity of Ni-BTC,[49] resulting in the decreased surface area of the resultant composites, which is consistent with the results of SEM images. Moreover, the successful preparation of Ni-BTC@GO hybrid composites is proved by the lower surface area of Ni-BTC@GO 2 than Ni-BTC.

The morphology of the GO, Ni-BTC, and Ni-BTC@GO 2 composites was further characterized by TEM. It can be observed that GO presents an irregular nanosheet layer structure, and the sheets are stacked together in disorder (Figure S4a). Meanwhile, Ni-BTC has a regular octahedral structure (Figure S4b), which is consistent with that observed in the SEM image. Through the TEM image of Ni-BTC@GO 2 (Figure S4c), it can be observed that in the composite material, the addition of GO did not influence the structure of
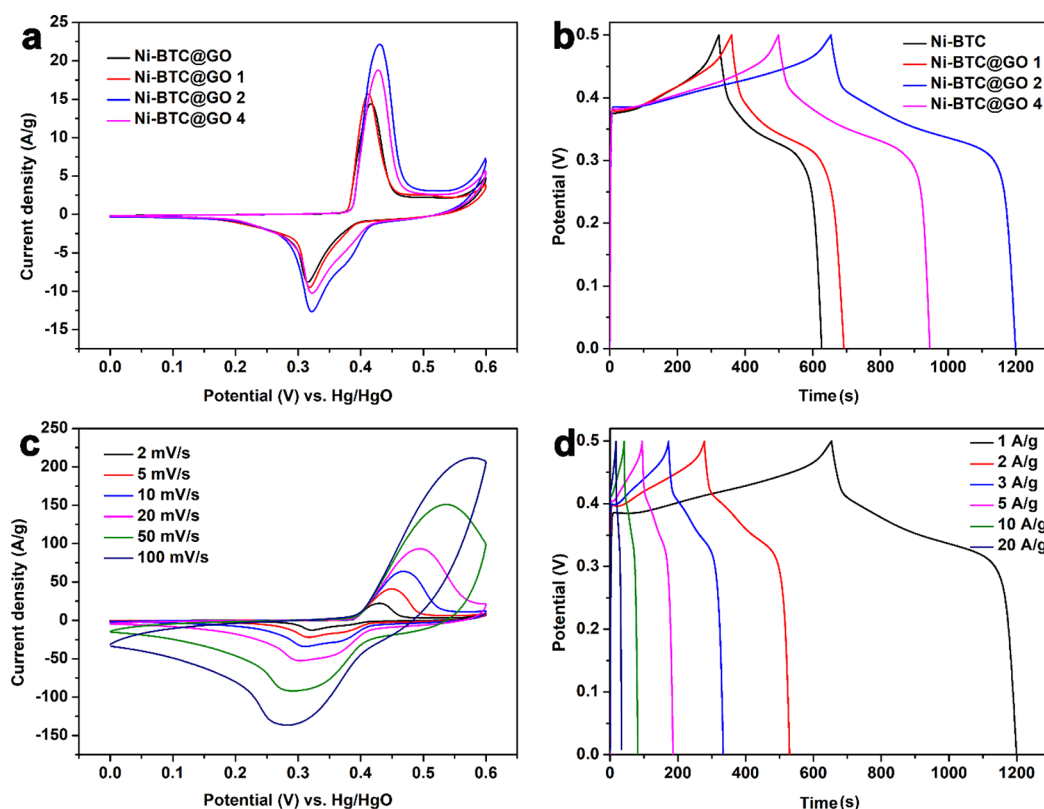
Figure 5. (a) CV curves of Ni-BTC and Ni-BTC@GO composites at 2 mV/s, (b) GCD curves of Ni-BTC and Ni-BTC@GO composites at 1 A/g, (c) CV curves of Ni-BTC@GO 2 at 2−100 mV/s, and (d) GCD curves of Ni-BTC@GO 2 at 1−20 A/g.

Ni-BTC, and the presence of Ni-BTC also made GO uniformly dispersed into single-layer sheets again and attached to the surface of Ni-BTC.

The thermostability and actual amount of GO in Ni-BTC@GO 2 could be evaluated by TG-DTG curves (Figure S5). The pristine GO suffers an apparent loss near 100 °C due to the loss of adsorbed water. Subsequently, the major mass loss of GO at about 200 °C accompanied by a vigorous release of gas is attributed to CO, CO_2, and steam release from labile functional groups. When the temperature is higher than 400 °C, the weight residue of pure GO is approximately 0%.[50] The Ni-BTC@GO composite shows almost the same trend as Ni-BTC, containing the desorption process of absorbed water (within 150 °C) and decomposition of the organic ligand (around 400 °C).[46] Notably, relatively lesser residues (i.e., Ni derivatives) of Ni-BTC@GO (17.9%) are observed than Ni-BTC (19.9%), which may be due to the additional weight losses of GO. According to the weight residues and relative Ni contents in Ni-BTC and the composite, it can be calculated that the actual loading of GO is approximately 10 wt % in the sample of Ni-BTC@GO 2.

XPS survey spectra of Ni-BTC and Ni-BTC@GO composites are depicted in Figure 4 and Figure S6. The binding states of C, O, and Ni elements are evaluated by deconvoluting the C1s, O1s, and Ni2p. The existence of O−C═O and C═C (derived from the organic ligand) in Ni-BTC is verified by the peaks at binding energies of 287.00 and 283.86 eV, respectively (Figure 4c).[51] The high-resolution O1s spectrum represents two dominant peaks at 532.17 and 530.50 eV, which are in line with C═O and metal−O bonds (Figure 4e).[52] In the Ni2p spectrum of Ni-BTC (Figure 4e), peaks at 877.80 and 860.23 (855.17) eV are assigned to Ni^{3+} and Ni^{2+},

respectively.[53] After being decorated with GO sheets, obvious shifts of C1s, O1s, and Ni2p peaks are obtained in the spectra of Ni-BTC@GO composites. Due to the existence of C and O elements in the raw GO sheet, the shift of C1s and O1s may result from the adulteration process. Compared with the Ni2p spectrum in the pristine Ni-BTC, a decreased binding energy of Ni2p1 (877.68, 877.77, and 877.66 eV in Ni-BTC@GO 1, 2, and 4, respectively) and increased binding energy of Ni2p3 (860.57 (855.35), 860.36 (855.31), and 860.55 (855.34) eV in Ni-BTC@GO 1, 2, and 4, respectively) are observed. Shifts of these binding energies indicate that the attachment of GO sheets on the surface of Ni-BTC is mainly in the manner of chemical bonding, instead of physical adsorption, which verifies the great stability of the as-prepared composites. Notably, compared with Ni-BTC@GO 1 and Ni-BTC@GO 4, Ni-BTC@GO 2 shows the most minute shift of binding energy in Ni2p, validating its stably morphologically retained property under the GO dosage of 0.02 g.

3.2. Electrochemical Analysis. CV (cyclic voltammetry) and GCD (galvanostatic charge−discharge) tests via a three-electrode system in an electrolyte of 3 M KOH were conducted to evaluate the electrochemical capacitance performances. The specific capacitance of GO was tested to be 180 F/g (Figure S7). Distinct redox peaks are observed instead of rectangular shapes in Figure 5a, indicating their typical pseudocapacitive behavior based on the reversible Faraday reaction of Ni^{2+} in electrolyte solution. The higher peak current of Ni-BTC@GO 2 is obtained compared to other electrodes, demonstrating that Ni-BTC@GO 2 has significantly enhanced electrochemical activity.[54,55] The integral area of the CV curve can directly reflect the capacitance performance. The order of the integrated area of the CV

Table 1. Comparison of the Electrochemical Performance of Similar MOF@GO Composites Reported in the Literature

| material	capacitance	rate capacitance	cycling performance	electrolyte	reference
Ni−Co−Cu−O	917.3 mF/cm^2	<42% (10−50 mA/cm^2)	83% retention after 2500 cycles	1 M KOH	62
G-NiS	409.2 F/g at 5 A/g	73.4% (5−20 A/g)	98.1% retention after 1000 cycles	3 M KOH	63
Co$_{0.4}$Ni$_{1.6}$P	330 F/g at 1 A/g	22.7% (1−10 A/g)	96% retention after 5000 cycles at 1 A/g	NA	64
spike-piece-structured Ni(OH)$_2$ interlayer nanoplates	2.83 F/cm^2 at 6 mA/cm^2	64.3% (6−24 mA/cm^2)	51.5% retention after 3000 cycles at 24 mA/cm^2	2 M KOH	65
Ni-MOF (H$_2$BDC, triethylenediamine)	804 F/g at 1 A/g	66% (1−10 A/g)	37.5% retention after 5000 cycles at 10 A/g	2 M KOH	35
nanoflower-like Ni-MOF (2-MeIm)	849 F/g at 1 A/g	66.4% (1−10 A/g)	83% retention after 5000 cycles at 5 A/g	6 M KOH	37
Ni-Co-MOF (2-MeIm)/GO	447.2 F/g at 1 A/g	61% (1−5 A/g)	99.6% retention after 300 cycles at 1 A/g	6 M KOH	39
2D/2D NiCo-MOF (PTA, TEA)/GO	413.61 C/g at 0.5 A/g	69.29% (1−20 A/g)	NA	2 M KOH	40
Ni-MOF (*p*-phthalic acid)/Ti$_3$C$_2$T$_x$	867.3 F/g at 1 A/g	64.4% (1−20 A/g)	87.1% retention after 5000 cycles at 5 A/g	2 M KOH	41
q-2D-MOF (H$_3$BTC)/rGO	292 F/g at 1 A/g	NA	>100% after 1000 cycles	1 M H$_2$SO$_4$	46
Ni-BTC (H$_3$BTC, 2-MeIm)@GO	1199 F/g at 1 A/g	68%	84.47% retention after 5000 cycles at 10 A/g	3 M KOH	this work

curves of these four electrodes is Ni-BTC < Ni-BTC@GO 1 < Ni-BTC@GO 4 < Ni-BTC@GO 2 (Figure 5a), which at the same time represents the order of their specific capacitance. This fact can also be demonstrated by the GCD curves at 1 A/g as shown in Figure 5b, where Ni-BTC@GO 2 has the longest charge/discharge time. Moreover, all GCD curves have obvious charging and discharging plateaus, again demonstrating their typical pseudocapacitive behavior. The specific capacitance can be calculated from the GCD curves by using eq S1.[56] The specific capacitances of Ni-BTC, Ni-BTC@GO 1, Ni-BTC@GO 2, and Ni-BTC@GO 4 are 625.6, 691.6, 1199, and 945.4 F/g, respectively. GO sheets on the surface can significantly improve the conductivity of Ni-BTC, reducing the ion transport path and increasing the specific capacitance. As the amount of GO increases, the charging and discharging time is first increasing followed by decreasing, which reveals that the GO dosage is unsaturated in Ni-BTC@GO 10, resulting in its weaker conductivity and specific capacitance than Ni-BTC@GO 20.

Excess GO dosage in Ni-BTC@GO 40, however, would lead to deteriorated GO aggregation and repressed conductivity performance, which are consistent with the results from SEM images. As shown in the SEM images, it can be observed that among Ni-BTC@GO 1, 2, and 4, the lamellar GO is tightly adhered to the surface of the octahedral Ni-BTC. In particular, in Ni-BTC@GO 2, the GO sheets are uniformly distributed on the Ni-BTC surface, while the excessive GO in Ni-BTC@GO 4 accumulates on the surface of the MOF, which may block the Ni ion transport path and, at the same time, hinder the contact between the MOF and the electrolyte. The charging/discharging behavior and capacitive behavior of the composite electrode are related to the synergistic effect of Ni-BTC and GO. GO can increase the conductivity of the composites and provide enough embedding/dis-embedding space of OH$^-$, while Ni-BTC can provide a uniform rigid framework for GO adhesion and reduce the aggregation of GO.

CV curves of Ni-BTC@GO 2 are shown in Figure 5c (the CV curves of other materials are shown in Figures S8a, S9a, and S10a; scan rates ranging from 2 to 100 mV/s). Ni-BTC@GO 2 shows more notable redox peaks, demonstrating a substantial increment in capacitance. The presence of redox peaks can be observed in the diagram, which indicates that the capacitance is actually a pseudocapacitance that is caused by the redox mechanism. Nickel-based MOFs (Ni-MOFs) for

supercapacitor applications are due to their ability to produce extremely high theoretical specific capacitance because they not only have a porous structure but also ample active sites that enhance the transfer of ions and variable oxidation state (Ni^{2+} and Ni^{3+}).[57] On the one hand, the electrochemical performance of the pristine Ni-BTC has been reported previously.[58] Peaks in the CV curve are mainly ascribed to the intercalation and desorption of OH$^-$ ions between MOF spheres during the reaction, where the metal nickel ion inside the MOF framework promotes the Faradaic redox reaction on the electrode/electrolyte interfaces.[59,60] On the other hand, due to the nonconductive character of GO, a composite surface covered by GO sheets is difficult for the electrostatic adsorption of charged species. Enhancement of the electrochemical property is due to the properties of GO in providing homogeneous product particles of desirable size and distribution. Benefiting from the addition of GO sheets, a larger surface area and higher accessibility of electrolyte ions are obtained.[61] As shown in the CV curves of Ni-BTC@GO composites (Figure 5 and Figures S9 and S10 in the paper), Ni-BTC@GO composites show similar redox peaks to the pristine Ni-BTC, indicating their similar pseudocapacitance mechanism to supercapacitor electrodes. A synergistic effect between Ni-BTC and GO sheets is obtained, indicating the effective role of GO sheets in the structural improvement of Ni-BTC by increasing the contact area between the electrode and the electrolyte, as well as shortening the diffusion path of ions and preserving the activate sites of Ni ions during the electrochemical test.

Due to the hysteresis kinetics of charge transfer caused by electrode polarization, the oxidation peaks of Ni-BTC@GO 2 move toward higher potentials and the reduction peaks are shifted to the lower voltage with the increase in scan rates.[55] Moreover, the shape of the CV curves remains consistent with increasing scan rate, which means that the Ni-BTC@GO 2 electrode has not only exceptional rate properties but also excellent cyclability. The GCD values of Ni-BTC@GO 2 were measured when the current density equals 1−20 A/g (Figure 5d) (GCD curves of other materials are displayed in Figures S2b, S3b, and S4b). Typical pseudocapacitive behavior is demonstrated by the apparent potential platform between 0 and 0.5 V in the GCD curves of Ni-BTC@GO 2. Ni-BTC@GO 2 shows good Coulombic efficiency, which could be indicated from the curves' symmetrical structure during the
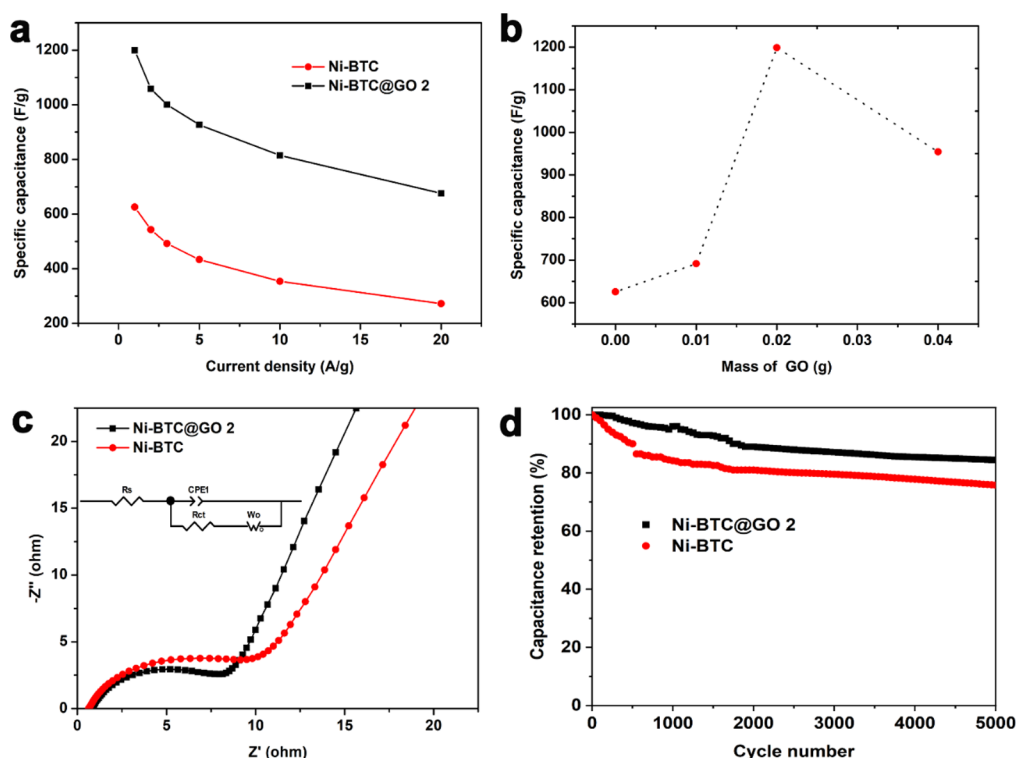
Figure 6. (a) Specific capacitance at various current densities of Ni-BTC and Ni-BTC@GO 2, (b) dependence of specific capacitance on the mass of GO at a current density of 1 A/g, (c) electrochemical impedance spectroscopy (EIS) of Ni-BTC and Ni-BTC@GO 2 in the frequency range of 0.01 Hz to 100 kHz, and (d) cycling performance of Ni-BTC and Ni-BTC@GO 2 at a current density of 1 A/g in 3 M KOH electrolyte.

rapid charge−discharge procedure. Specific capacitances obtained for Ni-BTC@GO 2 are 1199, 1058.6, 1000.8, 927, 815, and 676 F/g at 1, 2, 3, 5, 10, and 20 A/g, respectively. The specific capacitance of 1199 F/g at a current density of 1 A/g is the highest value compared with similar MOF@GO composites (Table 1).[35,37,39−41,46,62−65]

The specific capacitances at different current densities are illustrated in Figure 6a and Figure S10. The specific capacitances of Ni-BTC, Ni-BTC@GO 1, Ni-BTC@GO 2, and Ni-BTC@GO 4 are 354, 378, 815, and 621 F/g, respectively, at a current density of 10 A/g. As a result, these values indicate capacity retention values of 56.6, 54.7, 68.0, and 65.7%, respectively, compared to capacities of 625.6, 691.6, 1199, and 945.4 F/g at a current density of 1 A/g. The Ni-BTC@GO 2 electrode retains 56.4% of the capacity when the value of current density reaches 20 A/g, which means that the samples as-prepared at high current densities exhibit excellent electron mobility and ion diffusion. The rate performance of the Ni-BTC@GO 2 composite is better than that of other Ni-based materials and Ni@GO composites (Table 1). Figure 6b indicates the specific capacitance of the Ni-BTC@GO hybrid supercapacitor electrode versus the amount of GO, which is also affected by the amount of the Ni element. The GO amount and Ni elements in Ni-BTC@GO could affect the supercapacitor performance mainly from two aspects: (i) tuning the composite structure and morphology and (ii) influencing the amount of Ni active sites of pseudocapacitance. The Ni-BTC@GO 2 electrode exhibits the best charge and discharge duration and the maximum specific capacitance. A decrement of device performance is obtained in Ni-BTC@GO 4.

The frequency range of 0.01−100 kHz is tested for electrochemical impedance spectroscopy (EIS) data, and

Nyquist plots are shown in Figure 6c. The Nyquist plot includes semicircles and lines, which are located in high-frequency and low-frequency regions. Lines represent ion diffusion, which corresponds to the Warburg resistance (Z_w). The higher the line slope, the smaller the Z_w value. The slope of Ni-BTC@GO 2 is significantly higher than that of Ni-BTC. A schematic of the equivalent analog circuit with the materials is included in Figure 6c. According to the simulation results, the bulk electrolyte solution resistance (R_s) values of Ni-BTC and Ni-BTC@GO 2 are 0.6602 Ω and 0.7911 Ω, respectively. The semicircle diameter in the high-frequency region reveals charge transfer resistance (R_{ct}) induced by the redox behavior. Ni-BTC@GO 2 has the smallest semicircle diameter. The values of R_{ct} of Ni-BTC and Ni-BTC@GO 2 are 7.649 Ω and 7.065 Ω, and the corresponding electrical conductivities of Ni-BTC and Ni-BTC@GO 2 are 0.131 and 0.142 S/m, respectively. CPE represents the fixed-phase element of the equivalent circuit.[55,66,67] In summary, Ni-BTC@GO 2 exhibits high-performance impedance characteristics where the OH− ions in the electrolyte own faster diffusion capacity to the electrode surface. A simulated equivalent circuit can be obtained, and its main parameters (as shown in Table 2) are derived through numerical fitting.[68]

Table 2. Equivalent Circuit Parameters Obtained from EIS Plots of Ni-BTC and Ni-BTC@GO 2

	R_s (Ω)	R_{ct} (Ω)
Ni-BTC	0.7911	7.649
error (%)	1.5072	16.607
Ni-BTC@GO 2	0.6602	7.065
error (%)	1.8552	16.609
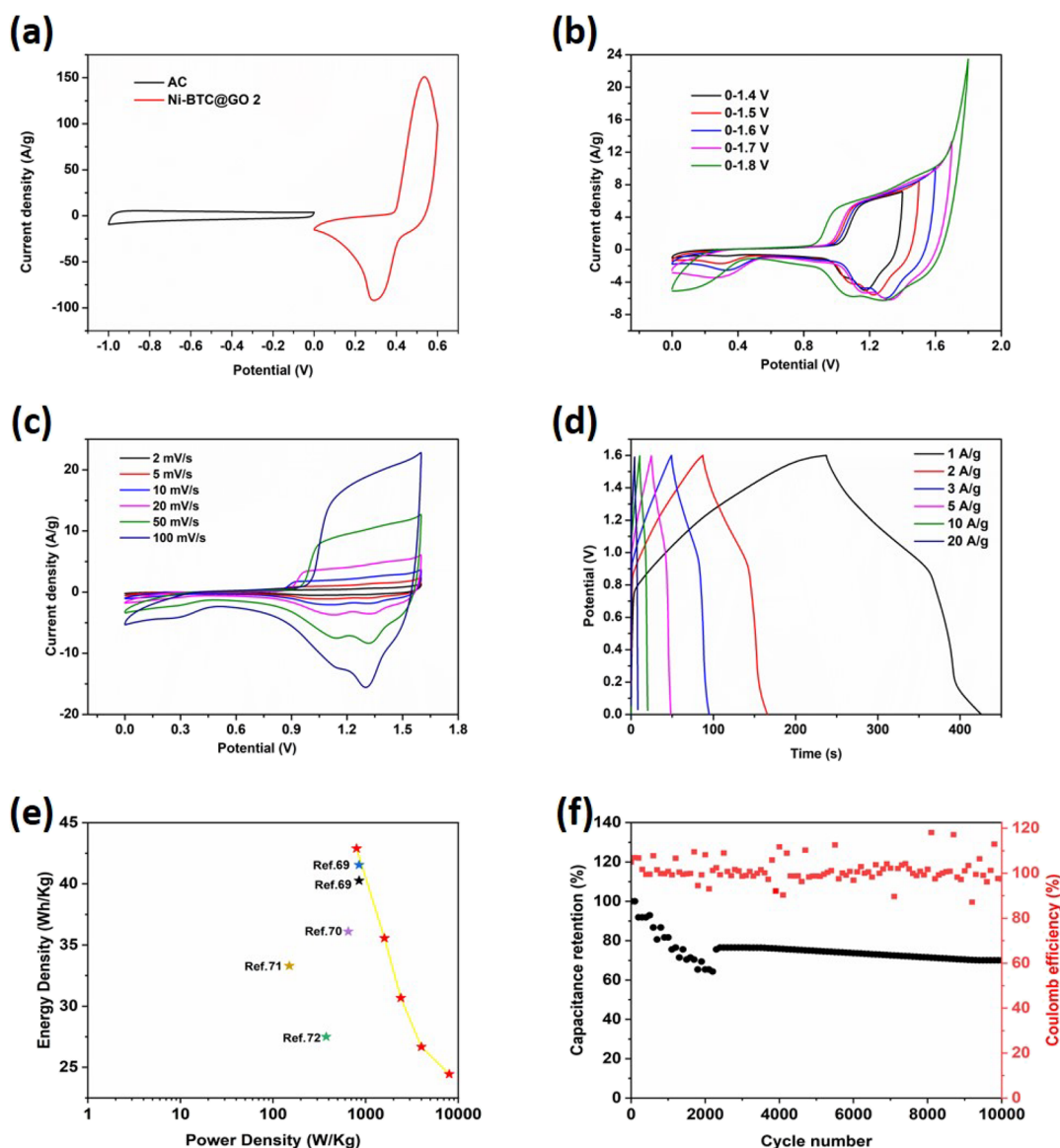
Figure 7. (a) CV windows for active C and Ni-BTC@GO 2 measured at 50 mV/s, (b) different operation windows measured at 50 mV/s, (c) CV curves at different scan rates, (d) GCD curves at different current densities, (e) Ragone plots of the ASC Ni-BTC@GO 2//AC compared with other works,[69−72] and (f) cycling performance at 10 A/g for 10,000 cycles.

To clarify the decay of the performance of the synthesized composites after multiple charge/discharge measurements, Ni-BTC@GO 2 has a cycling stability of 84.47% after 5000 cycles at 10 A/g (in the potential range of 0−0.5 V) as shown in Figure 5d. Fluctuations are observed at the beginning of the cycle, mainly because the materials are still in the activation stage. However, in the latter part of the cycle, these curves stabilize as the materials are fully activated. Finally, the capacity retention values of Ni-BTC and Ni-BTC@GO 2 are 81 and 89%, respectively, demonstrating that the Ni-BTC@GO 2 composite electrode has better stability than the Ni-BTC electrode and other Ni-based materials (Table 1). The excellent performance of Ni-BTC@GO 2 indicates that appropriate GO addition is important in the material performance. The most intuitive manifestation of different GO loadings is the variation in the surface as well as the structure of the material, which plays important roles in the electron transfer trajectory and speed, as well as the adequacy of electrolyte contact with the material. Due to the

functionalization of MOF with GO, the process of the insertion and de-insertion of OH⁻ leads to the reduction of the volume change of MOF, which improves the cycling performance of hybrid materials.

An ASC was fabricated by the Ni-BTC@GO 2 composite as a positive electrode to further evaluate its electrochemical properties. In this two-electrode cell, active C was used as the counter electrode and a 3 M KOH aqueous solution as the electrolyte. The CV window for active C is in the potential range of −1.0 to 0 V, while for the Ni-BTC@GO 2 composite, it is 0−0.6 V. For the as-fabricated ASC, the working window is chosen according to the CV curves measured at 50 mV/s (Figure 7b). This shows that the CV curve of the ASC managed to keep similar shapes within the voltage window of 0−1.6 V, which was selected as the testing voltage window for subsequent measurements. Figure 7c shows the CV curves of the ASC at different scan rates from 2 to 100 mV/s. There was no observable distortion, indicating excellent rate capability. This result coincided well with the GCD measurements. The

calculated capacities from the GCD curves showed a maximum energy density of 42.89 Wh/kg at a power density of 800 W/kg and held up to an energy density of 24.44 Wh/kg even at a power density as high as 7998 W/kg. To evaluate the electrochemical performance of the as-fabricated ASC, a comparison was made with a few recently reported analogues (Figure 7e). Ni-BTC@GO 2//AC exhibited properties superior to those of reported composites, such as NiCo-LDH@MOF//AC, NiCo-LDH//AC, Ni-Co LDH//AC, NiCo-LDH/10//CNT, and ZIF-67-LDH−CNP-110//AC. Last but not least, the cycling performance of Ni-BTC@GO 2//AC was assessed with 10,000 GCD cycles and 70% capacitance retention was achieved, indicating an outstanding stability.

4. CONCLUSIONS

In this study, enhancement of charge capacitance of Ni-BTC and avoidance of GO aggregation could be solved by the in situ synthesis of Ni-BTC@GO heterostructures, which proposes an effective strategy for the fabrication of high-performance supercapacitor electrodes. The 3D structure of Ni-BTC provides a rigid framework for 2D GO dispersion, reaching a synergistic effect on the electrochemical performances of the resultant nanostructured heterostructures. The Ni-BTC@GO heterostructure is superior to Ni-BTC in aspects of steric hindrance, electron transport, and ion diffusion rate. Specific capacitances of Ni-BTC, Ni-BTC@GO 1, Ni-BTC@GO 2, and Ni-BTC@GO 4 are 625.6, 691.6, 1199, and 945.4 F/g, respectively. The highest specific capacitance of Ni-BTC@GO 2 is obtained compared with reported MOF@GO composites. Notably, Ni-BTC@GO 2 owns satisfactory cycling performance, which retains 84.47% of the initial capacity compared to 75.81% for Ni-BTC even after 5000 cycles. The Ni-BTC@GO composite electrode material owns the capacity of both the mechanical strength and functional groups of GO and the 3D stereo structure of MOF. Greater GO dispersion that benefited from the rigid framework effect of Ni-BTC contributes to the trajectory and speed of electron transfer and the adequacy of electrolyte contact with the material during the electrochemical experiments. Moreover, the assembled asymmetric capacitor exhibits an energy density of 40.89 Wh/kg at 800 W/kg, and it still remains at 24.44 Wh/kg at 7998 W/kg. This work not only introduces an excellent electrode material for high-performance supercapacitors but also provides new insights for the fabrication of hybrid nanocomposites to enhance the conductivity performance in the future.

ASSOCIATED CONTENT

Supporting Information

The Supporting Information is available free of charge at https://pubs.acs.org/doi/10.1021/acsomega.2c07187.

Figures, tables, materials, synthesis methods, characterization, and electrochemical analysis (PDF)

AUTHOR INFORMATION

Corresponding Authors

Yaxiong Ji − *Hoffmann Institute of Advanced Materials, Shenzhen Polytechnic, Shenzhen 518055, P. R. China;* orcid.org/0000-0002-2201-2569; Email: kobejyx@126.com

Shifeng Wang − *Innovation Laboratory of Materials for Energy and Environment Technologies, Institute of Oxygen Supply, Tibet University, Lhasa 850000, P.R. China;* orcid.org/0000-0001-6169-2598; Phone: +86 15818696045; Email: wsf365@163.com

Authors

Tianen Chen − *Hoffmann Institute of Advanced Materials, Shenzhen Polytechnic, Shenzhen 518055, P. R. China; Innovation Laboratory of Materials for Energy and Environment Technologies, Institute of Oxygen Supply, Tibet University, Lhasa 850000, P.R. China*

Tao Shen − *Hoffmann Institute of Advanced Materials, Shenzhen Polytechnic, Shenzhen 518055, P. R. China*

Yuanhao Wang − *Hoffmann Institute of Advanced Materials, Shenzhen Polytechnic, Shenzhen 518055, P. R. China*

Zexu Yu − *Liaoning Machinery Research Institute Co., Ltd., Shenyang 110032, China*

Wei Zhang − *PetroChina Petrochemical Research Institute, Beijing 102206, China*

Yi Zhang − *Shanghai Soong Ching Ling School, Shanghai 200000, China*

Zeen Ouyang − *Guiyang No. 1 High School, Guizhou 550081, China*

Qingguo Cai − *Innovation Laboratory of Materials for Energy and Environment Technologies, Institute of Oxygen Supply, Tibet University, Lhasa 850000, P.R. China*

Complete contact information is available at:
https://pubs.acs.org/10.1021/acsomega.2c07187

Author Contributions

T.C.: methodology and original draft preparation; T.S.: methodology and review and editing; Y.W.: software; Z.Y.: validation; W.Z.: formal analysis; Y.Z.: investigation; Z.O.: data curation; Q.C.: data curation; Y.J.: conceptualization, resources, review and editing, and project administration; S.W.: conceptualization, visualization, supervision, and funding acquisition.

Notes

The authors declare no competing financial interest.

ACKNOWLEDGMENTS

REFERENCES

(1) Kalair, A.; Abas, N.; Saleem, M. S.; Kalair, A. R.; Khan, N. Role of Energy Storage Systems in Energy Transition from Fossil Fuels to Renewables. *Energy Storage* **2021**, *3*, No. e135.

(2) Singh, P.; Singh, S.; Kumar, G.; Baweja, P. *Energy: Crises, Challenges and Solutions*, First *Edition. Edited*; John Wiley & Sons 2021;

(3) Liu, G.; Lucas, M.; Shen, L. Rural Household Energy Consumption and Its Impacts on Eco-Environment in Tibet: Taking Taktse County as an Example. *Renew. Sust. Energ. Rev.* **2008**, *12*, 1890−1908.

(4) Jiang, D.; Hao, M.; Fu, J.; Zhuang, D.; Huang, Y. Spatialoral Variation of Marginal Land Suitable for Energy Plants from 1990 to 2010 in China. *Sci. Rep.* **2014**, *4*, 1.

(5) Zhang, Q.; Zeng, Z. R. Application and Development of Solar Street Lamp in China. *Appl. Mech. Mater.* **2015**, *734*, 952.

(6) Huibo, W.; Awan, R. U.; Qayyum, A.; Munir, A.; Khan, J.; Gulzar, F. How Financial Development Affects Green Energy Finance? Relationship between Environmental Regulation and Economic Performance. *Environ. Sci. Pollut. R.* **2022**, *29*, 14355−14370.

(7) Jin, X.; Du, S. Evaluation of Low-Carbon Competitiveness in Western China. *Acta Ecol. Sin.* **2013**, *33*, 1260−1267.

(8) Mehtab, T.; Yasin, G.; Arif, M.; Shakeel, M.; Korai, R. M.; Nadeem, M.; Muhammad, N.; Lu, X. Metal-Organic Frameworks for Energy Storage Devices: Batteries and Supercapacitors. *J. Energy Storage* **2019**, *21*, 632−646.

(9) Libich, J.; Máca, J.; Vondrák, J.; Čech, O.; Sedlaříková, M. Supercapacitors: Properties and Applications. *J. Energy Storage* **2018**, *17*, 224−227.

(10) Yao, B.; Zhang, J.; Kou, T.; Song, Y.; Liu, T.; Li, Y. Paper-Based Electrodes for Flexible Energy Storage Devices. *Adv. Sci.* **2017**, *4*, 1700107.

(11) Gao, Z.; Zhang, Y.; Song, N.; Li, X. Biomass-Derived Renewable Carbon Materials for Electrochemical Energy Storage. *Mater. Res. Lett.* **2017**, *5*, 69−88.

(12) Saikia, B. K.; Benoy, S. M.; Bora, M.; Tamuly, J.; Pandey, M.; Bhattacharya, D. A Brief Review on Supercapacitor Energy Storage Devices and Utilization of Natural Carbon Resources as Their Electrode Materials. *Fuel* **2020**, *282*, No. 118796.

(13) Wang, Z.; Li, H.; Tang, Z.; Liu, Z.; Ruan, Z.; Ma, L.; Yang, Q.; Wang, D.; Zhi, C. Hydrogel Electrolytes for Flexible Aqueous Energy Storage Devices. *Adv. Funct. Mater.* **2018**, *28*, 1804560.

(14) Peng, L.; Liang, Y.; Huang, J.; Xing, L.; Hu, H.; Xiao, Y.; Dong, H.; Liu, Y.; Zheng, M. Mixed-Biomass Wastes Derived Hierarchically Porous Carbons for High-Performance Electrochemical Energy Storage. *ACS Sustainable Chem. Eng.* **2019**, *7*, 10393−10402.

(15) Forouzandeh, P.; Kumaravel, V.; Pillai, S. C. Electrode Materials for Supercapacitors: A Review of Recent Advances. *Catalysts* **2020**, *10*, 969.

(16) Liang, J.; Jiang, C.; Wu, W. Toward Fiber-, Paper-, and Foam-Based Flexible Solid-State Supercapacitors: Electrode Materials and Device Designs. *Nanoscale* **2019**, *11*, 7041−7061.

(17) Lu, H.; Zhao, X. S. Biomass-Derived Carbon Electrode Materials for Supercapacitors. *Sustainable Energy Fuels* **2017**, *1*, 1265−1281.

(18) Wang, F.; Wu, X.; Yuan, X.; Liu, Z.; Zhang, Y.; Fu, L.; Zhu, Y.; Zhou, Q.; Wu, Y.; Huang, W. Latest Advances in Supercapacitors: From New Electrode Materials to Novel Device Designs. *Chem. Soc. Rev.* **2017**, *46*, 6816−6854.

(19) Yan, J.; Li, S.; Lan, B.; Wu, Y.; Lee, P. S. Rational Design of Nanostructured Electrode Materials toward Multifunctional Supercapacitors. *Adv. Funct. Mater.* **2020**, *30*, 1902564.

(20) An, C.; Zhang, Y.; Guo, H.; Wang, Y. Metal Oxide-Based Supercapacitors: Progress and Prospectives. *Nanoscale Adv.* **2019**, *1*, 4644−4658.

(21) Wang, Y.; Guo, J.; Wang, T.; Shao, J.; Wang, D.; Yang, Y. W. Mesoporous Transition Metal Oxides for Supercapacitors. *Nanomaterials* **2015**, *5*, 1677−1689.

(22) Yang, Z.; Ma, J.; Bai, B.; Qiu, A.; Losic, D.; Shi, D.; Chen, M. Free-Standing PEDOT/Polyaniline Conductive Polymer Hydrogel for Flexible Solid-State Supercapacitors. *Electrochim. Acta* **2019**, *322*, No. 134769.

(23) Yu, G.; Hu, L.; Liu, N.; Wang, H.; Vosgueritchian, M.; Yang, Y.; Cui, Y.; Bao, Z. Enhancing the Supercapacitor Performance of Graphene/MnO$_2$ Nanostructured Electrodes by Conductive Wrapping. *Nano Lett.* **2011**, *11*, 4438−4442.

(24) Yan, J.; Ma, Y.; Zhang, C.; Li, X.; Liu, W.; Yao, X.; Yao, S.; Luo, S. Polypyrrole-MXene Coated Textile-Based Flexible Energy Storage Device. *RSC Adv.* **2018**, *8*, 39742−39748.

(25) Hemanth, N. R.; Kandasubramanian, B. Recent Advances in 2D MXenes for Enhanced Cation Intercalation in Energy Harvesting Applications: A Review. *Chem. Eng. J.* **2020**, *392*, No. 123678.

(26) Wang, C.; Muni, M.; Strauss, V.; Borenstein, A.; Chang, X.; Huang, A.; Qu, S.; Sung, K.; Gilham, T.; Kaner, R. B. Graphene's Role in Emerging Trends of Capacitive Energy Storage. *Small* **2021**, *17*, 2006875.

(27) Huang, X.; Qi, X.; Boey, F.; Zhang, H. Graphene-Based Composites. *Chem. Soc. Rev.* **2012**, *41*, 666−686.

(28) Down, M. P.; Rowley-Neale, S. J.; Smith, G. C.; Banks, C. E. Fabrication of Graphene Oxide Supercapacitor Devices. *ACS Appl. Energy. Mater.* **2018**, *1*, 707−714.

(29) Mohd Abdah, M. A. A.; Zubair, N. A.; Azman, N. H. N.; Sulaiman, Y. Fabrication of PEDOT Coated PVA-GO Nanofiber for Supercapacitor. *Mater. Chem. Phys.* **2017**, *192*, 161−169.

(30) Davidson, J. A.; Jenkins, S. J.; Gorrec, F.; Clarke, S. M. 2D Constraint Modifies Packing Behaviour: A Halobenzene Monolayer with X3 Halogen-Bonding Motif. *Mol. Phys.* **2021**, *119*, No. E1900940.

(31) Zhang, J. L.; Niu, T. C.; Wee, A. T. S.; Chen, W. Self-Assembly of Binary Molecular Nanostructure Arrays on Graphite. *Phys. Chem. Chem. Phys.* **2013**, *15*, 12414−12427.

(32) Bi, S.; Banda, H.; Chen, M.; Niu, L.; Chen, M.; Wu, T.; Wang, J.; Wang, R.; Feng, J.; Chen; Dincă; Kornyshev; Feng, G. Molecular Understanding of Charge Storage and Charging Dynamics in Supercapacitors with MOF Electrodes and Ionic Liquid Electrolytes. *Nat. Mater.* **2020**, *19*, 552.

(33) Sheberla, D.; Bachman, J. C.; Elias, J. S.; Sun, C. J.; Shao-Horn, Y.; Dincă, M. Conductive MOF Electrodes for Stable Supercapacitors with High Areal Capacitance. *Nat. Mater.* **2017**, *16*, 220−224.

(34) Liu, Y.; Wang, Y.; Wang, H.; Zhao, P.; Hou, H.; Guo, L. Acetylene Black Enhancing the Electrochemical Performance of NiCo-MOF Nanosheets for Supercapacitor Electrodes. *Appl. Surf. Sci.* **2019**, *492*, 455−463.

(35) Gao, S.; Sui, Y.; Wei, F.; Qi, J.; Meng, Q.; He, Y. Facile Synthesis of Cuboid Ni-MOF for High-Performance Supercapacitors. *J. Mater. Sci.* **2018**, *53*, 6807−6818.

(36) Xiao, L.; Yao, S.; Liu, J.; Zou, H.; Xu, Y.; Cao, Y.; Chen, C. Efficient Ultrasonic Synthesis of Ni-Based Metal−Organic Framework for High Performance Battery-Type Supercapacitor Electrodes. *Energy Tecchnol.* **2022**, *10*, 2100350.

(37) Kale, A. M.; Manikandan, R.; Justin Raj, C.; Dennyson Savariraj, A.; Voz, C.; Kim, B. C. Protonated Nickel 2-Methylimidazole Framework as an Advanced Electrode Material for High-Performance Hybrid Supercapacitor. *Mater. Today Energy* **2021**, *21*, No. 100736.

(38) Zhao, F.; Liu, Y.; Hammouda, S. B.; Doshi, B.; Guijarro, N.; Min, X.; Tang, C. J.; Sillanpää, M.; Sivula, K.; Wang, S. MIL-101(Fe)/g-C$_3$N$_4$ for Enhanced Visible-Light-Driven Photocatalysis toward Simultaneous Reduction of Cr(VI) and Oxidation of Bisphenol A in Aqueous Media. *Appl. Catal. B* **2020**, *272*, No. 119033.

(39) Hong, J.; Park, S. J.; Kim, S. Synthesis and Electrochemical Characterization of Nanostructured Ni-Co-MOF/Graphene Oxide Composites as Capacitor Electrodes. *Electrochim. Acta* **2019**, *311*, 62−71.

(40) Li, S.; Shi, C.; Pan, Y.; Wang, Y. 2D/2D NiCo-MOFs/GO Hybrid Nanosheets for High-Performance Asymmetrical Supercapacitor. *Diamond Relat. Mater.* **2021**, *115*, No. 108358.

(41) Qu, Y.; Shi, C.; Cao, H.; Wang, Y. Synthesis of Ni-MOF/Ti3C2Tx Hybrid Nanosheets via Ultrasonific Method for Supercapacitor Electrodes. *Mater. Lett.* **2020**, *280*, No. 128526.

(42) Cheng, J.; Liu, K.; Li, X.; Huang, L.; Liang, J.; Zheng, G.; Shan, G. Nickel-Metal-Organic Framework Nanobelt Based Composite Membranes for Efficient Sr^{2+} Removal from Aqueous Solution. *Environ. Sci. Ecotechnol.* **2020**, *3*, No. 100035.

(43) Gan, Q.; Liu, B.; Zhao, K.; He, Z.; Liu, S. Flower-like NiCo$_2$O$_4$ from Ni-Co 1,3,5-Benzenetricarboxylate Metal Organic Framework Tuned by Graphene Oxide for High-Performance Lithium Storage. *Electrochim. Acta* **2018**, *279*, 152−160.

(44) Hummers, W. S., Jr.; Offeman, R. E. Preparation of Graphitic Oxide. *J. Am. Chem. Soc.* **1958**, *80*, 1339.

(45) Wang, L.; Wu, Y.; Cao, R.; Ren, L.; Chen, M.; Feng, X.; Zhou, J.; Wang, B. Fe/Ni Metal-Organic Frameworks and Their Binder-Free Thin Films for Efficient Oxygen Evolution with Low Overpotential. *ACS Appl. Mater. Interfaces* **2016**, *8*, 16736−16743.

(46) Ehrnst, Y.; Ahmed, H.; Komljenovic, R.; Massahud, E.; Shepelin, N. A.; Sherrell, P. C.; Ellis, A. V.; Rezk, A. R.; Yeo, L. Y. Acoustotemplating: Rapid Synthesis of Freestanding Quasi-2D MOF/Graphene Oxide Heterostructures for Supercapacitor Applications. *J. Mater. Chem. A Mater.* **2022**, *10*, 7058−7072.

(47) Chen, T.; Yang, A.; Zhang, W.; Nie, J.; Wang, T.; Gong, J.; Wang, Y.; Ji, Y. Architecting Nanostructured Co-BTC@GO Composites for Supercapacitor Electrode Application. *Nanomaterials* **2022**, *12*, 3234.

(48) Pryjomska-Ray, I.; Zornik, D.; Pätzel, M.; Krause, K. B.; Grubert, L.; Braun-Cula, B.; Hecht, S.; Limberg, C. Comparing Isomeric Tridentate Carbazole-Based Click Ligands: Metal Complexes and Redox Chemistry. *Chem. − Eur. J.* **2018**, *24*, 4858.

(49) Bao, L.; Nguyen, T.; Fei, H.; Sapurina, I.; Ngwabebhoh, A.; Bubulinca, C.; Munster, L.; Bergerova, E.; Lengalova, A.; Jiang, H.; Dao, T.; Bugraova, N.; Omastova, M.; Kazantseva, N.; Saha, P. Electrochemical performance of composites made of rGO with Zn-MOF and PANI as electrodes for supercapacitors. *Electrochim. Acta* **2021**, *367*, 137563.

(50) Zhang, L.; He, Y.; Feng, S.; Zhang, L.; Zhang, L.; Jiao, Z.; Zhan, Y.; Wang, Y. Preparation and tribological properties of novel boehmite/graphene oxide nano-hybrid. *Ceram. Int.* **2016**, *42*, 6178−6186.

(51) Kshetri, T.; Khumujam, D. D.; Singh, T. I.; Lee, Y. S.; Kim, N. H.; Lee, J. H. Co-MOF@MXene-Carbon Nanofiber-Based Freestanding Electrodes for a Flexible and Wearable Quasi-Solid-State Supercapacitor. *Chem. Eng. J.* **2022**, *437*, No. 135338.

(52) Wang, J.; Gong, J.; Zhang, H.; Lv, L.; Liu, Y.; Dai, Y. Construction of Hexagonal Nickel-Cobalt Oxide Nanosheets on Metal-Organic Frameworks Based on MXene Interlayer Ion Effect for Hybrid Supercapacitors. *J. Alloys Compd.* **2021**, *870*, No. 159466.

(53) Yang, X.; Tian, Y.; Li, S.; Wu, Y. P.; Zhang, Q.; Li, D. S.; Zhang, S. Heterogeneous Ni-MOF/V2CTx-MXene Hierarchically-Porous Nanorods for Robust and High Energy Density Hybrid Supercapacitors. *J. Mater. Chem. A Mater.* **2022**, *10*, 12225−12234.

(54) van Ngo, T.; Moussa, M.; Tung, T. T.; Coghlan, C.; Losic, D. Hybridization of MOFs and Graphene: A New Strategy for the Synthesis of Porous 3D Carbon Composites for High Performing Supercapacitors. *Electrochim. Acta* **2020**, *329*, No. 135104.

(55) Zheng, S.; Zhou, H.; Xue, H.; Braunstein, P.; Pang, H. Pillared-Layer Ni-MOF Nanosheets Anchored on Ti_3C_2 MXene for Enhanced Electrochemical Energy Storage. *J. Colloid Interface Sci.* **2022**, *614*, 130−137.

(56) Li, L.; Peng, S.; Wu; Yu, L.; Madhavi, S.; Lou, X. W. A Flexible Quasi-Solid-State Asymmetric Electrochemical Capacitor Based on Hierarchical Porous V_2O_5 Nanosheets on Carbon Nanofibers. *Adv. Energy Mater.* **2015**, *5*, 1500753.

(57) Khokhar, S.; Anand, H.; Chand, P. Current advances of nickel based metal organic framework and their nanocomposites for high performance supercapacitor applications: A critical review. *J. Energ. Storage* **2022**, *56*, No. 105897.

(58) Kang, L.; Sun, S.; Bin Kong, L.; Lang, J.; Luo, Y. Investigating metal-organic framework as a new pseudo-capacitive material for supercapacitors. *Chin. Chem. Lett.* **2014**, *25*, 957−961.

(59) Yang, J.; Zheng, C.; Xiong, P.; Li, Y.; Wei, M. Zn-doped Ni-MOF material with a high supercapacitive performance. *J. Mater. Chem. A* **2014**, *2*, 19005.

(60) Yan, H.; Bai, J.; Wang, J.; Zhang, X.; Wang, B.; Liu, Q.; Liu, L. Graphene homogeneously anchored with $Ni(OH)_2$ nanoparticles as advanced supercapacitor electrodes. *Cryst. Eng. Commun.* **2013**, *15*, 10007.

(61) Ibrahim, I.; Zheng, S.; Foo, C.; Huang, N.; Lim, H. Hierarchical nickel-based metal-organic framework/graphene oxide incorporated graphene nanoplatelet electrode with exceptional cycling stability for coin cell and pouch cell supercapacitors. *J. Enery. Storage* **2021**, *43*, No. 103304.

(62) Lin, L.; Li, X.; Huang, Y.; Sun, H. Synthesizing Ni-based ternary metal compounds for battery-supercapacitor hybrid devices with and without using nickel precursors. *Mat. Sci. Semicon. Proc.* **2019**, *98*, 81−89.

(63) Syganya, G.; Kalpana, G. Investigation of graphene based NiS nanocomposite by solvothermal method for energy storage application. *Mater. Lett-X.* **2021**, *12*, No. 100112.

(64) Nie, S.; Yang, H.; Zhou, C.; Liu, Y.; Pan, C.; Luo, J.; Ma, C.; Wang, Y. Bimetallic $Co_{0.4}Ni_{1.6}P$ derived from cobalt functionalized a new nickel metal-organic-framework as an advanced electrode for high-performance supercapacitors. *Inorg. Chem. Commun.* **2021**, *130*, No. 108733.

(65) Wu, L. C.; Chen, Y. J.; Mao, M. L.; Li, Q. H.; Zhang, M. Facile synthesis of spike-piece-structured $Ni(OH)_2$ interlayer nanoplates on nickel foam as advanced pseudocapacitive materials for energy storage. *ACS Appl. Mater. Interfaces* **2014**, *6*, 5168−5174.

(66) Zhu, G.; He, Z.; Chen, J.; Zhao, J.; Feng, X.; Ma, Y.; Fan, Q.; Wang, L.; Huang, W. Highly Conductive Three-Dimensional MnO2-Carbon Nanotube-Graphene-Ni Hybrid Foam as a Binder-Free Supercapacitor Electrode. *Nanoscale* **2014**, *6*, No. 04495e.

(67) Ramachandran, R.; Saranya, M.; Velmurugan, V.; Raghupathy, B. P. C.; Jeong, S. K.; Grace, A. N. Effect of Reducing Agent on Graphene Synthesis and Its Influence on Charge Storage towards Supercapacitor Applications. *Appl. Energy* **2015**, *153*, 22−31.

(68) Zhang, Y.; Lin, B.; Sun, Y.; Han, P.; Wang, J.; Ding, X.; Zhang, X.; Yang, H. MoO2@Cu@C Composites Prepared by Using Polyoxometalates@Metal-Organic Frameworks as Template for All-Solid-State Flexible Supercapacitor. *Electrochim. Acta* **2016**, *188*, 490−498.

(69) Chen, S.; Yu, D.; Li, G.; Jin, Y.; Yan, W. Construction of interconnected NiCo layered double hydroxides/metal-organic frameworks hybrid nanosheets for high-performance supercapacitor. *J. Energy Storage* **2022**, *48*, No. 103961.

(70) Ramachandran, R.; Lan, Y.; Xu, Z.-X.; Wang, F. Construction of NiCo-Layered Double Hydroxide Microspheres from Ni-MOFs for High-Performance Asymmetric Supercapacitors. *ACS Appl. Energy Mater.* **2020**, *3*, 6633−6643.

(71) Xiao, Z.; Bao, Y.; Li, Z.; Huai, X.; Wang, M.; Liu, P.; Wang, L. Construction of Hollow Cobalt−Nickel Phosphate Nanocages through a Controllable Etching Strategy for High Supercapacitor Performances. *ACS Appl. Energy Mater.* **2019**, *2*, 1086−1092.

(72) Wang, P.; Li, Y.; Li, S.; Liao, X.; Sun, S. Water-promoted zeolitic imidazolate framework-67 transformation to Ni−Co layered double hydroxide hollow microsphere for supercapacitor electrode material. *J. Mater. Sci.: Mater. Electron.* **2017**, *28*, 9221−9227.